

On Model Space Sampling in ADMIRE for Image Quality and Computational Efficiency

Siegfried Schlunk

Department of Biomedical Engineering
Vanderbilt University
Nashville, TN, USA
siegfried.g.schlunk@vanderbilt.edu

Brett Byram

Department of Biomedical Engineering
Vanderbilt University
Nashville, TN, USA

Abstract—Image quality and computational efficiency of the aperture domain model image reconstruction (ADMIRE) method is dependent on the specific model used. This makes it important for users to understand how various model design considerations could have significant impacts on image processing. In this work, we consider how undersampling, randomization of physical locations, and dimensionality reduction with independent component analysis (ICA) can be used to improve runtime. Specifically, we observed that undersampling resulted in a trade-off between contrast and efficiency, random sampling led to improved CNR, and ICA generally showed improved contrast and computation time.

Index Terms—ADMIRE, model, beamforming, ICA, random sampling

I. INTRODUCTION

Since the introduction of aperture domain model image reconstruction (ADMIRE) [1]–[3] further work has been focused in two areas: improving the algorithm to enhance image quality such as in the case of iterative ADMIRE [4], [5] and expanded model ADMIRE [6], and improving the efficiency of the algorithm such as with dimension reducing methods [7] or GPU-based implementations [8]–[10] to achieve real-time performance.

While these efforts have pushed the bounds of what ADMIRE is capable of, we had not up to this point conducted a formal analysis of how the specific model creation process may have an impact on the resulting image quality and how that balances with the computational load required. In this work, we focus on how the physical model parameters might be tuned in order to balance both quality and runtime, and start moving towards a general recommendation for most scenarios. We analyze various kinds of model undersampling, the impact of randomizing model predictor locations, and how dimensionality reduction using independent component analysis (ICA) performs compared to these other methods.

II. BEAMFORMING ALGORITHMS

A. Aperture Domain Model Image Reconstruction (ADMIRE)

Aperture domain model image reconstruction (ADMIRE) is a method for removing reverberation and off-axis clutter, and suppressing wavefront aberration. Byram et al. presented a detailed explanation of the components of the algorithm [2], and additional information can be found elsewhere [1], [3].

First we divide the delayed channel data into overlapping windows along the axial dimension, along which a short-time Fourier transform (STFT) is performed. For each primary frequency component, a physics-based model is created to decompose the observed aperture domain signals. This model matrix, X , contains the predicted aperture domain signals corresponding to some set of physical locations throughout the field-of-view of the transducer. This allows us to represent a given aperture domain signal, y , by its component sources, β , by

$$y = X\beta, \quad (1)$$

where y is for a specific wave number k and location (x_n, z_n) , X is the set of physical model predictors, and β the set of solved model coefficients. Due to the ill-posed nature of the problem, ADMIRE uses the elastic-net regularization technique [11] with the optimization equation

$$\hat{\beta} = \arg \min_{\beta} (||y - X\beta||^2 + \lambda(\alpha||\beta||_1 + (1 - \alpha)||\beta||_2^2/2)), \quad (2)$$

where $||\beta||_1$ is the L1 norm, $||\beta||_2$ is the L2 norm, and α is set between 0 and 1 to control the weighting between L1 and L2. λ is a regularization parameter which controls the degrees of freedom [12]. Here, we choose $\alpha = 0.9$ and $\lambda_{\text{LDF}} = (0.00189)y_{\text{RMS}}$ based on the root mean square (RMS) of the signal y .

Solving 2 gives us an estimate of β , which reveals the specific physical locations and relative amplitudes of the various signals that linearly combine to form y . ADMIRE then chooses some small region of interest (ROI) centered at the target location and can simply remove the coefficients for sources outside of that ROI, and reconstruct the decluttered signal as

$$y_{\text{decluttered}} = X\beta_{\text{ROI}}, \quad (3)$$

using only the coefficients β_{ROI} corresponding to signals originating from inside the ROI.

Once the aperture domain signal has been decluttered, the inverse STFT is applied to return to the time domain [13]. This results in a decluttered version of the channel data that can still be processed using other beamformers.

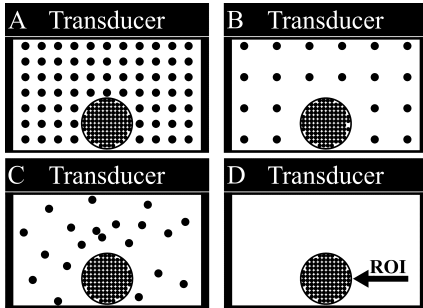


Fig. 1. Example models for use with ADMIRE. (A) Normal Base Model, (B) half-sampled model, (C) half-sampled with random locations, (D) ROI only model. Note that these are visual examples, and not representative of actual region sizes.

B. ADMIRE Model Variations

The ADMIRE model is composed of two distinct parts: the ROI and everything else. The ROI is a highly sampled section that represents our “good” signal components, those that we want to keep, while the everything else part is more sparsely sampled and represents possible sources of clutter, such as reverberation and off-axis sources. Fig. 1A shows a visual representation of what the Base Model of ADMIRE might look like, where the ROI is much more densely sampled compared to everywhere else in the imaging space.

1) *Undersampling*: When choosing the locations of our imaging space to be included in the model, we consider the axial and lateral limits and choose some degree of sampling to create a grid, as shown in Fig. 1A. Therefore, a simple way for us to reduce the number of predictors, and therefore improve computation time, is to reduce the sampling in those dimensions, creating a more sparsely sampled grid. For example, a half-sampled case as shown in Fig. 1B. In the extreme, we can completely remove the sparse section of the model leaving only the ROI, like in Fig. 1D. This would provide the absolute smallest model without considering further reducing the sampling in the ROI itself.

Additionally, model creation actually considers a third “dimension” in addition to just the axial and lateral physical dimensions. For every physical location (x_n, z_n) we additionally consider some number of possible phase offsets to account for possible variations in the phase of the returning echo. Therefore, we can additionally reduce the sampling of the phase offsets considered, which impacts all physical locations, including those in the ROI. For reference, we refer to the standard, default model as “Base Model” and the ROI only model as “ROI” in the results section. Further, sampling variations are denoted with “samp/X” and “phase/X” to indicate undersampling the physical locations and phase, respectively, by some ratio X.

2) *Randomization*: Randomization here refers to choosing the physical locations randomly rather than in a strict grid pattern. For example, Fig. 1C shows a variation of Fig. 1B where the number of predictors outside of the ROI are the same, but the locations have been randomly assigned. For this variation we only consider the physical locations in the sparse

region of the model, so there is no random version of the ROI only model, and there is no randomization of the phase offsets. Critically, because model generation occurs for each location and frequency, the model is randomly generated every time and the random locations change over the course of the image. We prefer this method rather than choosing a specific set of random locations for an entire image to reduce the chance of generating a particularly obtuse model that causes issues, and instead allowing the randomness to average out over the course of a full image. Variations where randomization is applied are denoted with “Rand”.

3) *Independent Component Analysis (ICA)*: Independent component analysis has been previously investigated by our group [7] as a means of dimensionality reduction. The process allows us to remove higher order correlations among our signals [14], [15], leaving us with a much smaller set of independent components. Our previous work tested several different ICA implementations and we decided to move forward with the fourth-order blind identification (FOBI) algorithm [15], [16]. This ICA method can be used to reduce the dimensionality of any arbitrary model, allowing ADMIRE to both run faster and require less of a memory footprint, which is critical for GPU-based, real-time versions of ADMIRE [8]–[10]. We include ICA compression in this work as a comparison to the other model variations since they seek to accomplish similar goals. Variations where ICA is used to reduce the dimensionality are denoted with “ICA”.

III. METHODS

A. Anechoic Cyst Phantoms

We used Field II [17], [18] to simulate n=6 5mm anechoic cysts. The simulation parameters are detailed in Table I. We additionally created noise cases for reverberation clutter (0dB signal-to-clutter ratio, SCR) and for thermal noise (0dB signal-to-noise ratio, SNR). The reverberation clutter was created as in previous work [19], [20]. For each phantom and each ADMIRE model variation, the contrast ratio and contrast-to-noise ratio (CNR) were calculated by

$$\text{contrast ratio} = 20\log_{10}\left(\frac{\mu_{\text{ROI}}}{\mu_{\text{background}}}\right) \quad (4)$$

$$\text{CNR} = \frac{|\mu_{\text{ROI}} - \mu_{\text{background}}|}{\sqrt{\sigma_{\text{ROI}}^2 + \sigma_{\text{background}}^2}}, \quad (5)$$

where μ is the mean value and σ is the standard deviation calculated from the enveloped, but not log compressed, data.

B. *in vivo* Kidney Case

We additionally included a simple *in vivo* kidney case captured with a Verasonics Vantage Ultrasound System (Verasonics, Inc., Kirkland, WA) with a C52 curvilinear transducer to compare against the simulations. We additionally computed the total runtime of the elastic-net regularization and compared that to the number of predictors in the model used for a chosen region of the image. The same region was used for all cases and the computation occurred on the same hardware to enable

TABLE I

FIELD II SIMULATION PARAMETERS FOR CONTRAST TARGET PHANTOMS

Parameter	Value
Number of elements	117
Number of mathematical elements (lateral)	7
Number of mathematical elements (elevation)	11
Element height	4 mm
Element width	0.254 mm
Kerf	0.003 mm
Lateral pitch	0.257 mm
Center frequency (f_c)	3 MHz
Sampling frequency (simulation) (f_s)	640 MHz
Sampling frequency (downsampled) (f_s)	40 MHz
Bandwidth	60%
Transmit focal depth	3 cm
Transmit/receive f-number	1

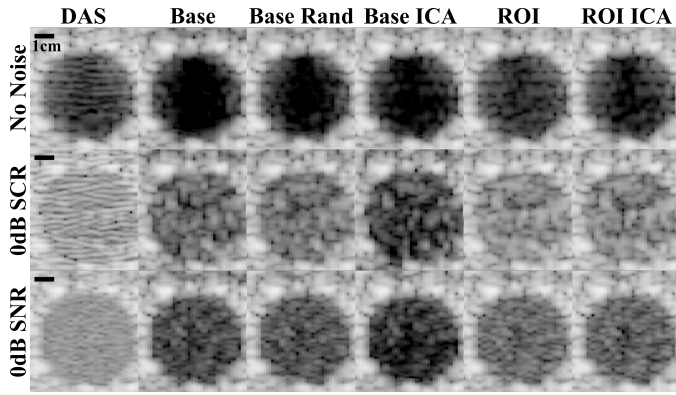


Fig. 2. B-mode images on an 60 dB dynamic range for an example anechoic cyst (no noise, 0dB SCR reverberation clutter, and 0dB SNR thermal noise) processed with DAS and various ADMIRE model variations. Base refers to the default Base Model ADMIRE, Base Rand is that same model but with predictor locations randomized, Base ICA is that same model after ICA dimensionality reduction, ROI is the ROI only model, and ROI ICA is the ROI only model after ICA dimensionality reduction.

fair comparison. This allowed us to get a general sense of how the reduced model size may improve computational efficiency.

IV. RESULTS

Fig. 2 shows a sample realization of a 5mm anechoic cyst for a selection of the more interesting model variations that we tested, and Table II and Table III list the measured contrast ratio and CNR for all tested variations. General trends in the data suggest that the ROI only model has image statistics very similar to DAS, and undersampling allows us some control over the degree of ADMIRE processing. In particular, highly sampled models had worse CNR but much better contrast ratio, while undersampling resulted in better CNR similar to DAS but less contrast ratio. Generally, our results indicated that reducing phase sampling had relatively little impact on image quality, and served as a relatively free computational boost. Randomization led to a consistent small improvement in CNR with relatively little impact on contrast ratio in all cases. Finally, ICA dimensionality reduction generally had similar or improved contrast ratio in all cases, and likewise had equivalent or better CNR compared to the non-reduced model

TABLE II
MEAN CONTRAST RATIO FOR ANECHOIC CYST SIMULATIONS

Added Noise	Contrast Ratio (dB)		
	None	0dB SCR	0dB SNR
DAS	-32.2±1.0	-12.1±0.6	-14.3±0.7
Base Model	-44.3±1.3	-21.5±1.6	-30.0±1.1
Base Rand	-41.3±1.2	-19.7±1.4	-28.1±1.0
Base ICA	-42.8±1.5	-27.3±1.7	-34.8±1.3
Base phase/4	-41.9±1.5	-20.6±1.5	-28.9±1.0
Base phase/4 ICA	-42.9±1.7	-27.5±1.7	-35.0±1.2
Base samp/4	-33.1±1.2	-16.3±1.2	-23.8±0.9
Base samp/4 Rand	-34.9±1.3	-15.4±0.9	-23.7±0.9
Base samp/4 phase/4	-33.2±1.4	-16.2±1.2	-23.8±0.9
ROI	-34.4±1.3	-15.5±1.0	-23.2±1.0
ROI ICA	-37.6±1.5	-16.4±1.1	-25.1±0.9
ROI phase/4	-34.8±1.3	-15.7±1.0	-23.6±1.0
ROI phase/4 ICA	-37.4±1.5	-16.3±1.1	-25.0±0.9

TABLE III
MEAN CNR FOR ANECHOIC CYST SIMULATIONS

Added Noise	Contrast-to-Noise Ratio (CNR)		
	None	0dB SCR	0dB SNR
DAS	6.1±0.6	3.5±0.8	4.7±0.5
Base Model	5.2±0.6	3.8±0.8	4.8±0.7
Base Rand	5.6±0.7	4.3±0.8	5.3±0.6
Base ICA	6.0±0.6	3.5±0.7	5.3±0.6
Base phase/4	5.4±0.6	3.9±0.7	5.0±0.6
Base phase/4 ICA	6.0±0.6	3.5±0.7	5.3±0.6
Base samp/4	5.7±0.6	4.0±0.7	5.3±0.6
Base samp/4 Rand	5.8±0.6	4.3±0.8	5.7±0.6
Base samp/4 phase/4	6.1±0.6	4.1±0.7	5.4±0.6
ROI	5.9±0.6	4.2±0.7	5.1±1.3
ROI ICA	6.2±0.6	4.3±0.8	5.8±0.6
ROI phase/4	6.0±0.6	4.2±0.7	5.5±0.6
ROI phase/4 ICA	6.2±0.6	4.3±0.8	5.7±0.6

equivalent except in the 0dB SCR reverberation clutter case where CNR was slightly lowered. In all variants of ADMIRE, the cyst results indicate that ADMIRE is still able to reduce or remove the majority of the added reverberation or thermal noise, based on the change in the speckle appearance inside and outside of the cyst.

The highlights of the *in vivo* kidney images are shown in Fig. 3. Here we see a continuation of the trends observed in the simulated data. ICA produces an image with stronger contrast ratio compared to both Base Model ADMIRE and DAS. We additionally see that the randomization that improved CNR in the cysts manifests as a slight smoothing of the speckle texture, improving the visibility of some structures. The runtime calculations are shown in Table IV, and are based on the time it took to process a single STFT window (all frequencies and locations). We get significantly improved computation time as we reduce the number of model predictors, although there is clearly processing overhead that starts to take over as the number of predictors shrink. Another interesting note is that ICA is substantially less efficient per predictor compared to any other model, though is still overall significantly faster than using the full Base Model. This is likely due to the ICA model matrix being a dense set of independent components, whereas the normal models naturally have a large amount of sparsity.

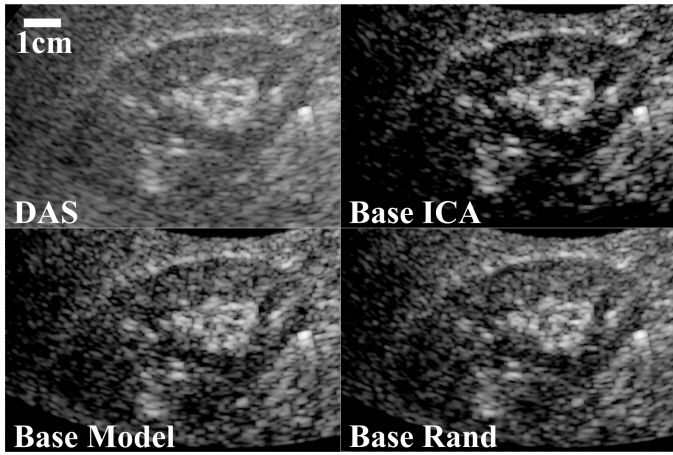


Fig. 3. B-mode images on an 60 dB dynamic range for an *in vivo* kidney processed with DAS, Base Model ADMIRE, Base Model after ICA dimensionality reduction, and Base Model with predictor locations randomized.

TABLE IV
RUNTIME CALCULATIONS FOR VARIATIONS

# Predictors	Total Time (sec)	Time/Predictor (sec)
Base Model	27574	67.343
Base phase/4	7070	0.00245
Base ICA	156	0.05412
ROI	235	0.01632
ROI phase/4	60	0.01490
ROI ICA	235	0.01612

Considering the ICA reduced models are “optimized” versions of the normal models, it is reasonable to expect they will have more information packed into an equivalent number of predictors, resulting in somewhat increased computation time per predictor.

V. DISCUSSION AND CONCLUSIONS

The results indicate that ICA reduction of the full Base Model is probably the best “universal” suggestion that can be made, providing equivalent or better image quality with a significant runtime improvement. ICA on the smaller models is still an improvement, but the benefits are substantially lower. However, all the undersampled variations including the ROI only model did still provide good noise reduction with similar CNR to normal DAS, which may be valuable for certain applications. Finally, randomizing the model predictor locations does not provide any improvement to runtime efficiency, but does result in a consistent improvement to CNR that may improve general image quality with no extra processing required.

ACKNOWLEDGMENT

The authors would like to thank the staff of the Vanderbilt University ACCRE computing resource. This work was supported by NIH grants R01EB020040 and S10OD023680-01, and additionally by NSF award IIS-1750994.

REFERENCES

- [1] B. Byram and M. Jakovljevic, “Ultrasonic Multipath and Beamforming Clutter Reduction: A Chirp Model Approach,” *IEEE Transactions on Ultrasonics, Ferroelectrics, and Frequency Control*, vol. 61, no. 3, pp. 428–440, 2014.
- [2] B. Byram, K. Dei, J. Tierney, and D. Dumont, “A Model and Regularization Scheme for Ultrasonic Beamforming Clutter Reduction,” *IEEE Transactions on Ultrasonics, Ferroelectrics, and Frequency Control*, vol. 62, no. 11, pp. 1913–1927, 2015.
- [3] K. Dei and B. Byram, “The Impact of Model-Based Clutter Suppression on Cluttered, Aberrated Wavefronts,” *IEEE Transactions on Ultrasonics, Ferroelectrics, and Frequency Control*, vol. 64, no. 10, pp. 1450–1464, 2017.
- [4] S. Schlunk, K. Dei, and B. Byram, “Iterative ADMIRE for High Dynamic Range B-Mode,” *IEEE International Ultrasonics Symposium (IUS)*, vol. 2018-Octob, pp. 1–4, 2018.
- [5] ———, “Iterative model-based beamforming for high dynamic range applications,” *IEEE Transactions on Ultrasonics, Ferroelectrics, and Frequency Control*, pp. 1–1, 2020. [Online]. Available: <https://ieeexplore.ieee.org/document/9149929/>
- [6] S. Schlunk and B. Byram, “Expanded beamforming models for high dynamic range scenarios,” *IEEE International Ultrasonics Symposium, IUS*, vol. 2020-Septe, no. Mv, pp. 21–24, 2020.
- [7] K. Dei, S. Schlunk, and B. Byram, “Computationally Efficient Implementation of Aperture Domain Model Image Reconstruction,” *IEEE Transactions on Ultrasonics, Ferroelectrics, and Frequency Control*, vol. 66, no. 10, pp. 1546–1559, 10 2019. [Online]. Available: <https://ieeexplore.ieee.org/document/8746209/>
- [8] C. Khan, K. Dei, and B. Byram, “A GPU-Based Implementation of ADMIRE,” in *2019 IEEE International Ultrasonics Symposium (IUS)*, vol. 2019-Octob. IEEE, 10 2019, pp. 1501–1504. [Online]. Available: <https://ieeexplore.ieee.org/document/8925842/>
- [9] C. Khan, K. Dei, S. Schlunk, K. Ozgun, and B. Byram, “Real-Time, Simultaneous DAS, ADMIRE, and SLSC Imaging Using GPU-Based Processing,” in *2020 IEEE International Ultrasonics Symposium (IUS)*. IEEE, 9 2020, pp. 1–4. [Online]. Available: <https://ieeexplore.ieee.org/document/9251587/>
- [10] ———, “A Real-Time, GPU-Based Implementation of Aperture Domain Model Image REconstruction,” *IEEE Transactions on Ultrasonics, Ferroelectrics, and Frequency Control*, vol. 3010, no. c, pp. 1–1, 2021.
- [11] H. Zou and T. Hastie, “Regularization and variable selection via the elastic net,” *Journal of the Royal Statistical Society: Series B (Statistical Methodology)*, vol. 67, no. 2, pp. 301–320, 2005.
- [12] R. J. Tibshirani and J. Taylor, “Degrees of Freedom in Lasso Problems,” *The Annals of Statistics*, vol. 40, no. 2, pp. 1198–1232, 2012.
- [13] B. Yang, “A Study of Inverse Short-Time Fourier Transform,” *IEEE International Conference on Acoustics, Speech and Signal Processing*, pp. 3541–3544, 2008.
- [14] J. Wang and C. I. Chang, “Independent component analysis-based dimensionality reduction with applications in hyperspectral image analysis,” *IEEE Transactions on Geoscience and Remote Sensing*, vol. 44, no. 6, pp. 1586–1600, 2006.
- [15] J. Shlens, “A Tutorial on Independent Component Analysis,” vol. 94043, pp. 1–13, 2014. [Online]. Available: <http://arxiv.org/abs/1404.2986>
- [16] J. F. Cardoso, “Source separation using higher order moments,” *ICASSP, IEEE International Conference on Acoustics, Speech and Signal Processing - Proceedings*, vol. 4, pp. 2109–2112, 1989.
- [17] J. A. Jensen, “Field: A Program for Simulating Ultrasound Systems,” *Paper presented at the 10th Nordic-Baltic Conference on Biomedical Imaging Published in Medical & Biological Engineering and Computing*, vol. 34, pp. 351–353, 1996.
- [18] J. A. Jensen and N. B. Svendsen, “Calculation of Pressure Fields from Arbitrarily Shaped, Apodized, and Excited Ultrasound Transducers,” *IEEE Transactions on Ultrasonics, Ferroelectrics, and Frequency Control*, vol. 39, pp. 262–267, 1992.
- [19] B. Byram and J. Shu, “Pseudononlineair ultrasound simulation approach for reverberation clutter,” *Journal of Medical Imaging*, vol. 3, no. 4, 2016.
- [20] ———, “A pseudo non-linear method for fast simulations of ultrasonic reverberation,” *Medical Imaging 2016: Ultrasonic Imaging and Tomography*, vol. 9790, no. April 2016, pp. 1–7, 2016.